Supporting Information

Electrochemical hydrogen generation by four-coordinate square-planar Ni(II) complex with N_2P_2-type ligand

Hidenori Miyake,[a] Satomi Hirasawa,[a] Yurika Uno,[a] Kenichi Nakao,[a] Takuma Kato,[a] Yuko Wasada-Tsutsui,[a] Yoshikuni Hara,[a] Tomohiro Ozawa,[a] Tomohiko Inomata,[a] and Hideki Masuda[a,b*]

[a]*Department of Life Science and Applied Chemistry, Graduate School of Engineering, Nagoya Institute of Technology, Gokiso-cho, Showa-ku, Nagoya 466-8555, Japan.*
[b]*Department of Applied Chemistry, Faculty of Engineering, Aichi Institute of Technology, 1247 Yachigusa, Yakusa-cho, Toyota 470-0392, Japan.*

Contents

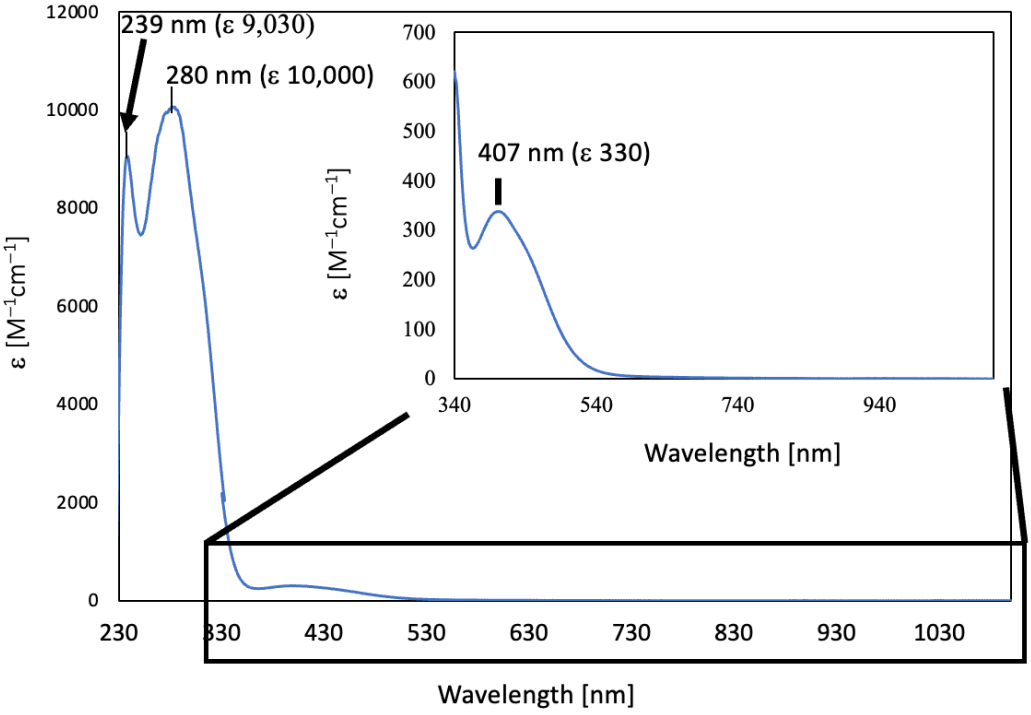

Fig. S1. UV-vis spectrum (230 ~ 1030 nm) of $[Ni(L_H)_2](BF_4)_2$ (1.0 mM) in CH_2Cl_2.

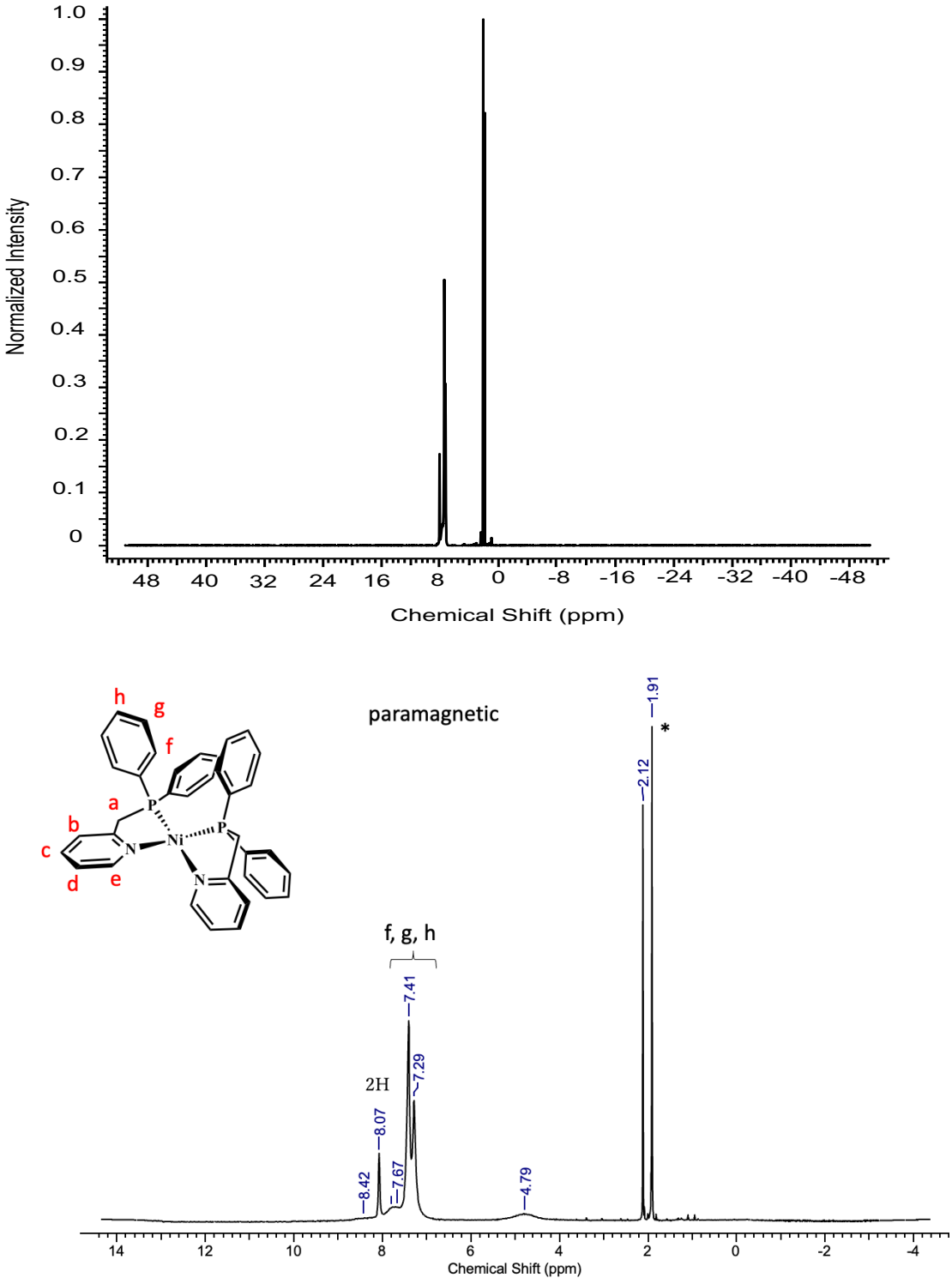

Fig. S2. ^{1}H-NMR spectrum of complex **1** (1.0 mM) in MeCN-d_3. (Upper) Wide and (below) normal ranges. Attribution of NMR spectra of paramagnetic species is very difficult and their peak intensities are not meaningful to discuss. It is beyond the scope of this study and were therefore not attributed.

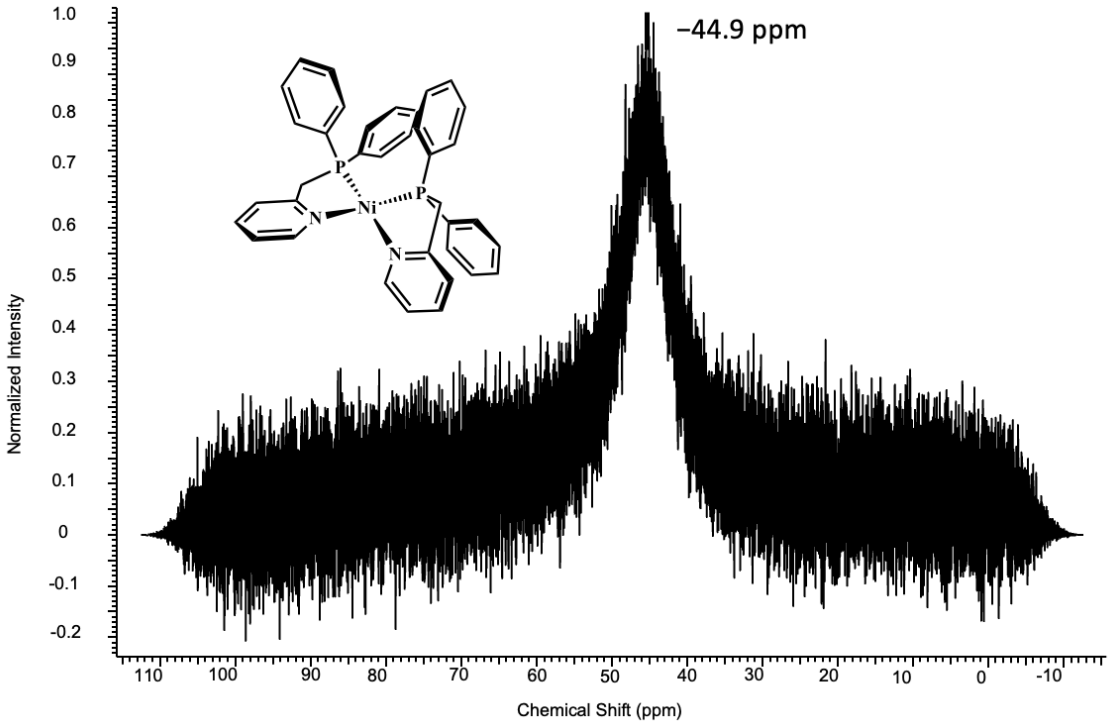

Fig. S3. $^{31}P\{^{1}H\}$ NMR spectrum of complex **1** (1.0 mM) in MeCN-d_3.

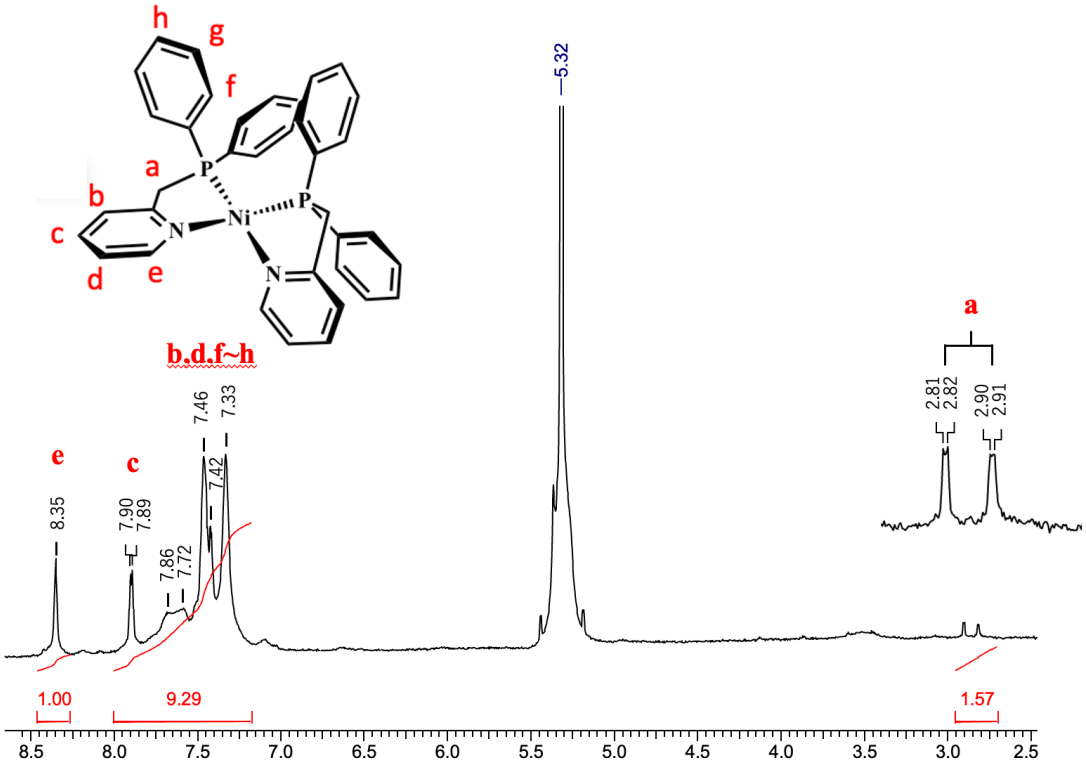

Fig. S4. ^{1}H-NMR spectrum of complex **1** (1.0 mM) in CD_2Cl_2. (Upper) Wide and (below) normal ranges.

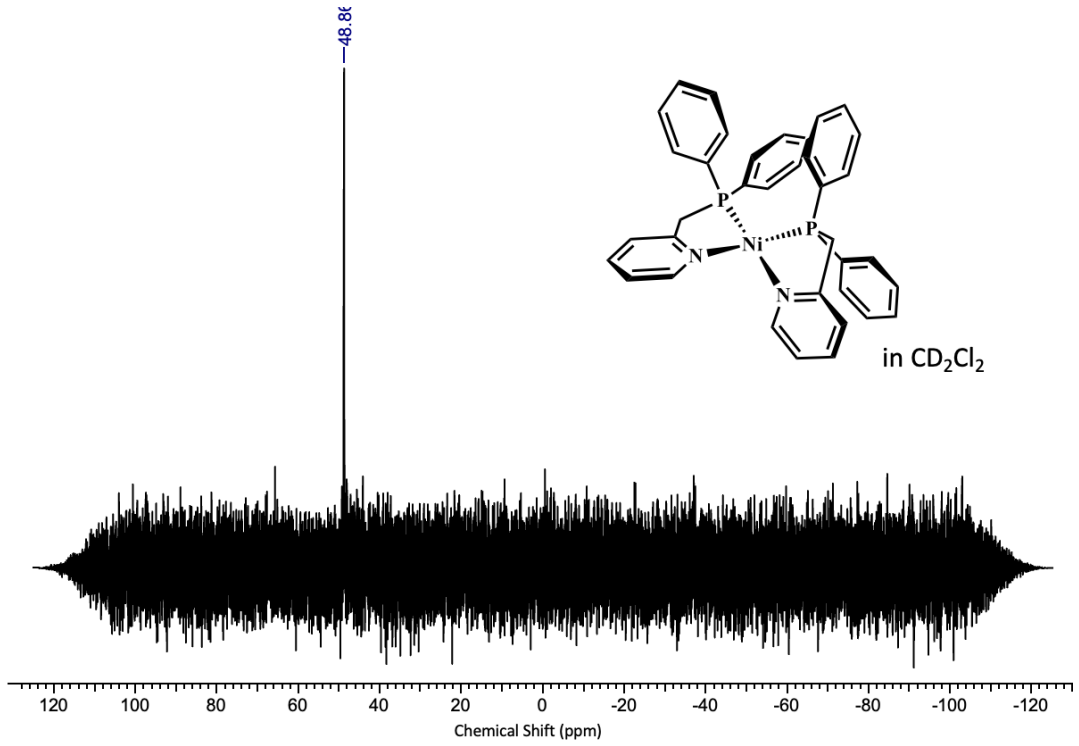

Fig. S5. ^{31}P{^{1}H} NMR spectrum of complex **1** (1.0 mM) in CD_2Cl_2.

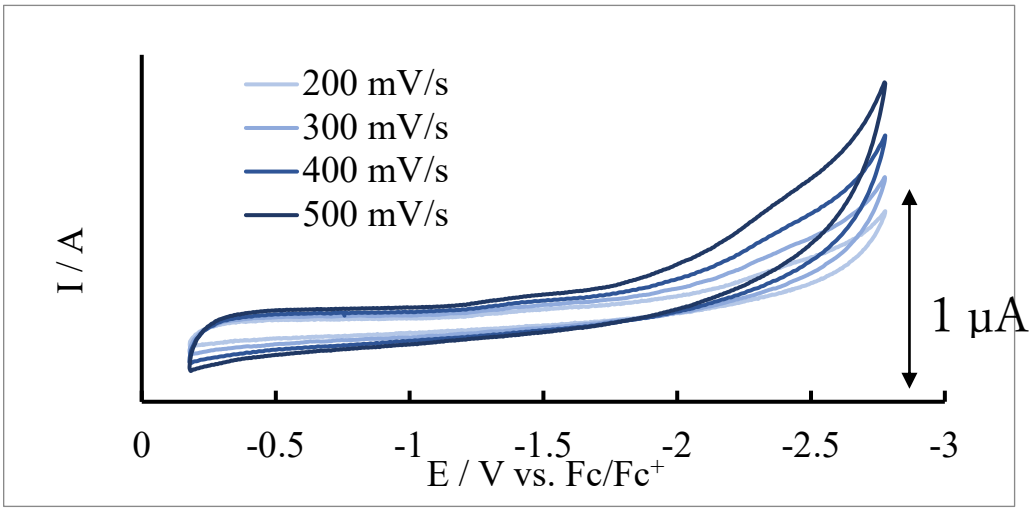

Fig. S6. CV of ligand L_H in the range of 0 ~ –2.7 V in MeCN, measured at several sweep rates under the same measurement conditions as complex **1**.

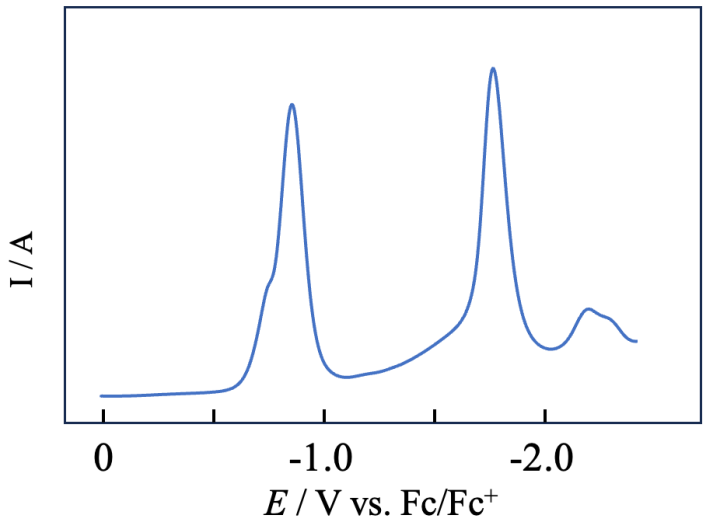

Fig. S7. DPV of $[Ni(L_H)_2](BF_4)_2$ in MeCN as measured under the same condition as CV.

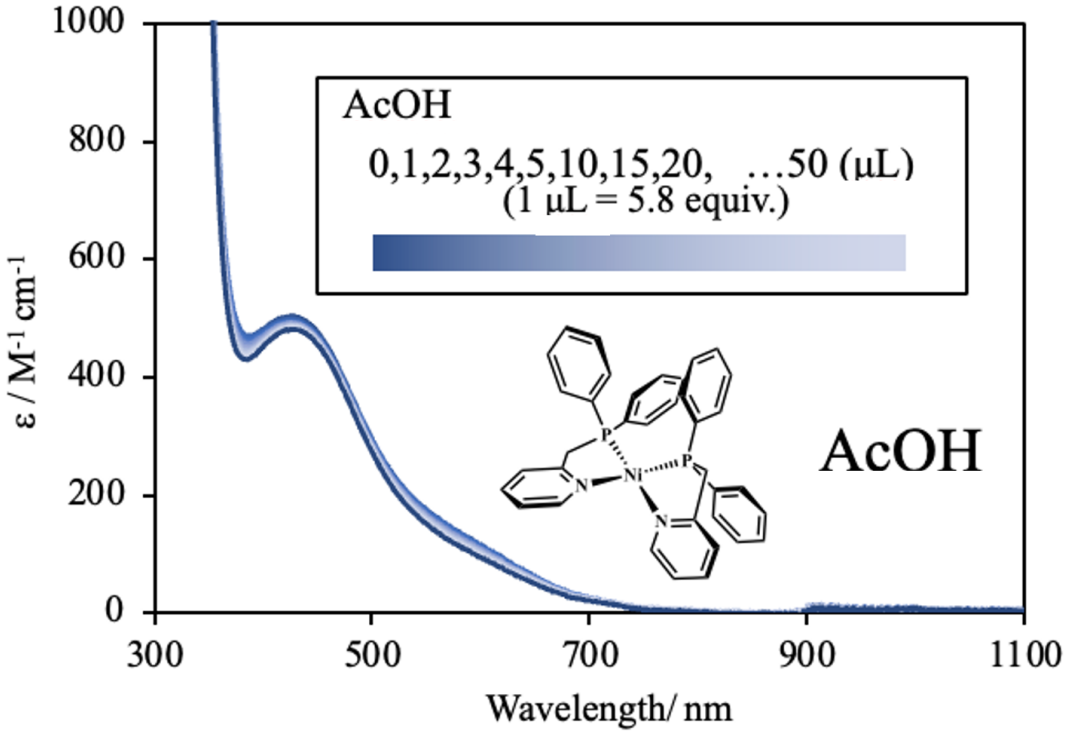

Fig. S8. UV-vis spectra of complex **1** (1.0 mM) in the presence (0 ~ 50 μL (290 equiv.)) of AcOH in MeCN.

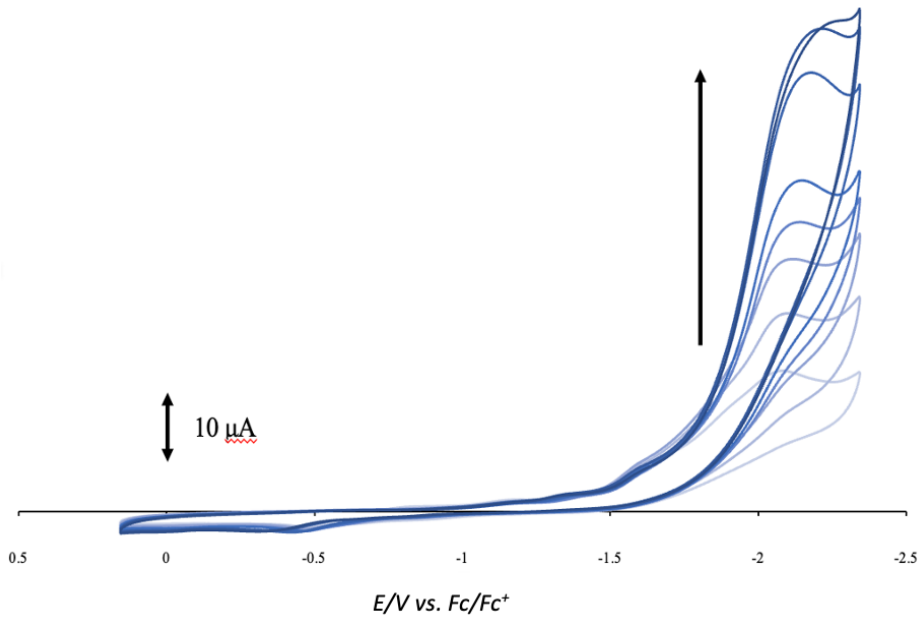

Fig. S9(a) CVs of complex **1** (1.0 mM) in MeCN containing 0.1 M TBAP in the presence of 0 - 203 equiv. of AcOD at room temperature under Ar atmosphere, recorded at a scan rate of 500 mV/s.

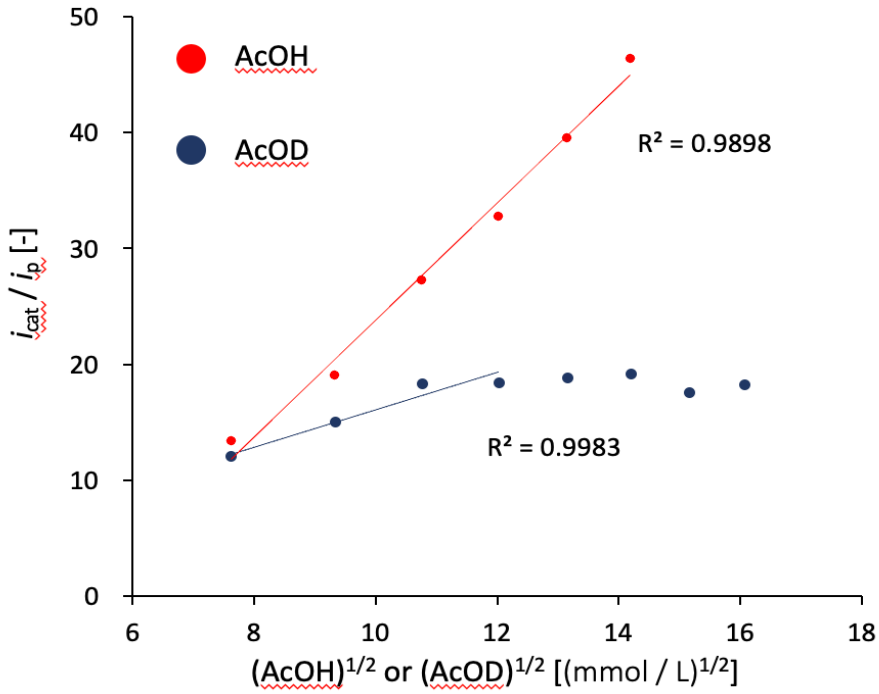

Fig. S9(b). Plots of i_{cat}/i_p *m*A vs. (AcOH or AcOD)$^{1/2}$/(mmol/L)$^{1/2}$ for complex **1** (1.0 mM) in the presence of 0 - 203 equiv. of AcOH or AcOD in MeCN containing 0.1 M TBAP at room temperature under Ar atmosphere, recorded at a scan rate of 500 mV/s.

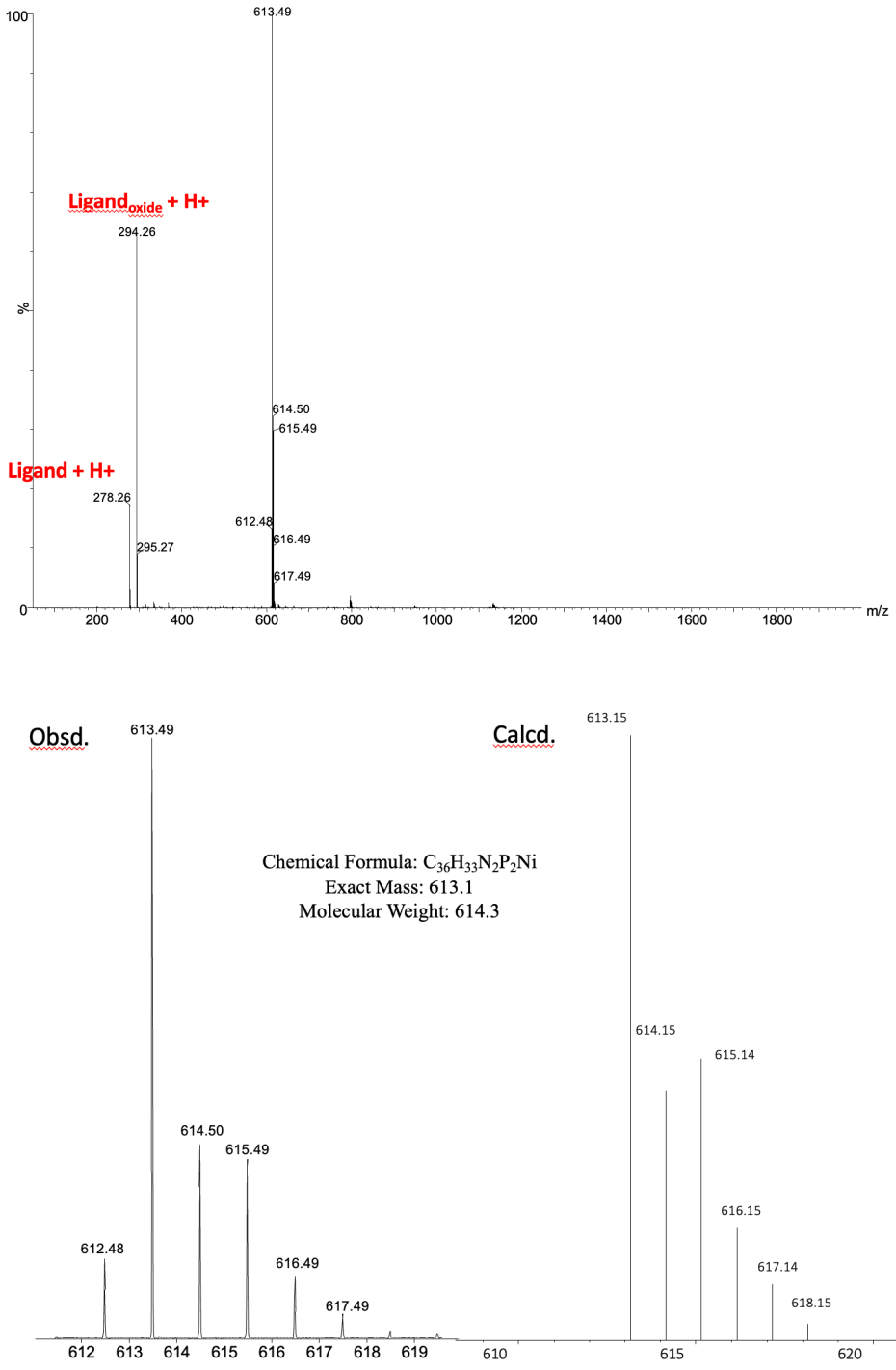

Fig. S10. ESI-MS spectrum (in the positive mode) of the solution prepared from the reaction of $Ni^0(COD)_2$, L_H and NH_4PF_6 in THF at –90 °C under anaerobic condition. The wide range (top) and local range and its simulation (bottom) assignable to ion cluster of $[Ni^{II}H(L_H)_2]^+$.

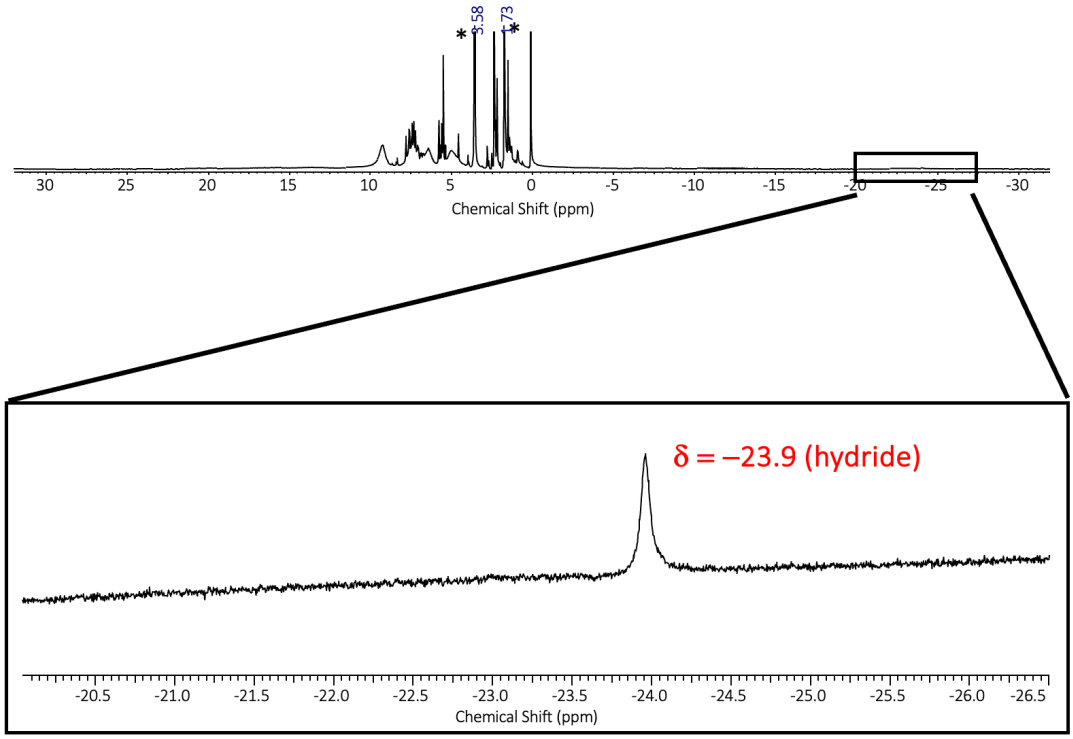

Fig. S11. ^{1}H NMR spectrum of the products obtained by the reaction of $Ni^{0}(COD)_2$ with NH_4PF_6 in THF-d_8 at –90 °C in degassed NMR sample tube.

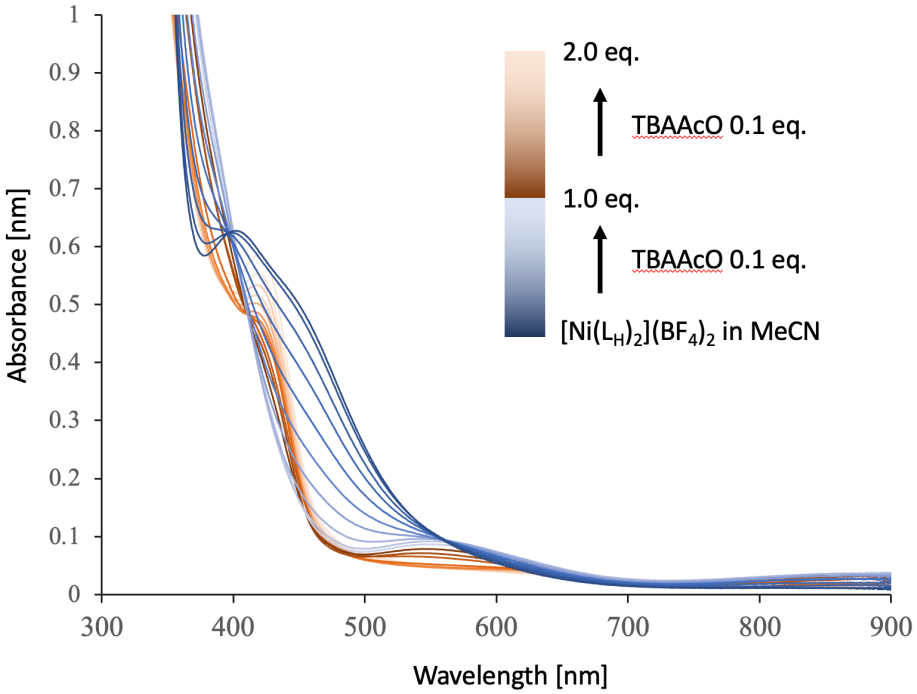

Fig. S12. UV-vis spectra of complex **1** (0.1 mM) in the presence of 0 – 2.0 equiv. of $TBA^{+}AcO^{-}$ in MeCN at room temperature under Ar atmosphere.

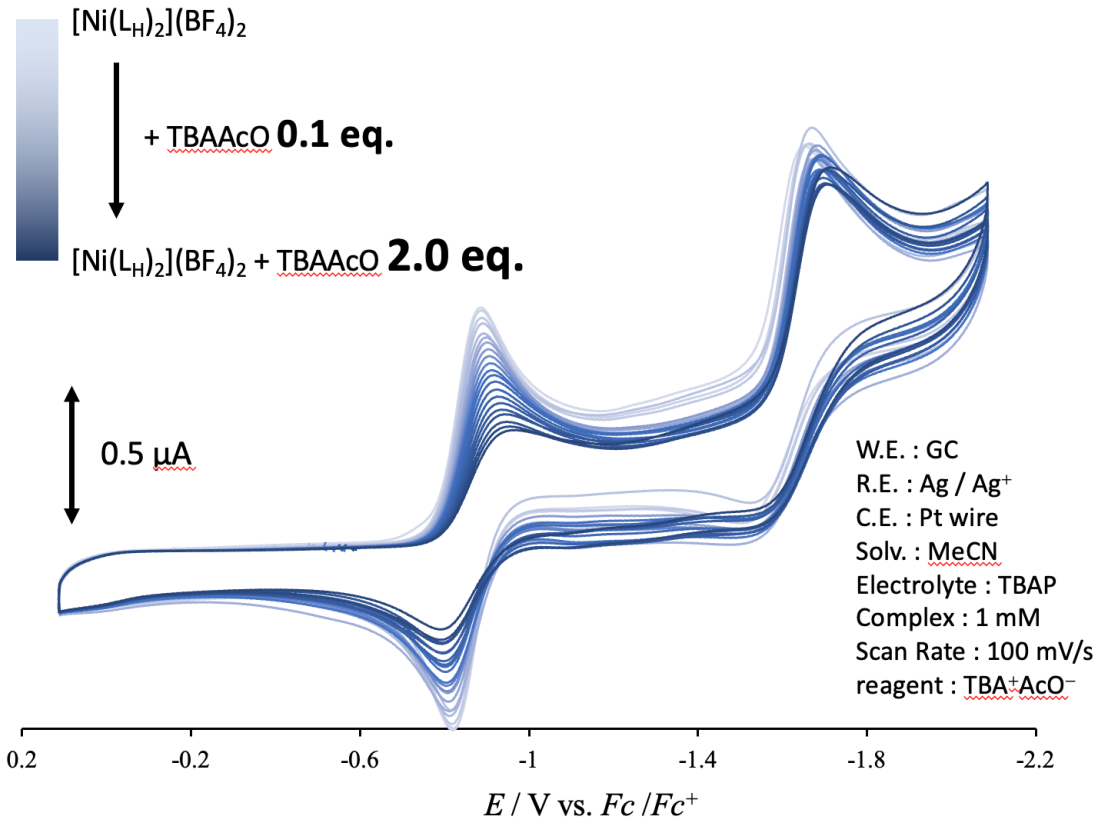

Fig. S13. CVs of complex **1** (1.0 mM) in MeCN containing 0.1 M TBAP in the presence of 0 – 2.0 equiv. of $TBA^{+}AcO^{-}$ at room temperature under Ar atmosphere, recorded at a scan rate of 100 mV/s.

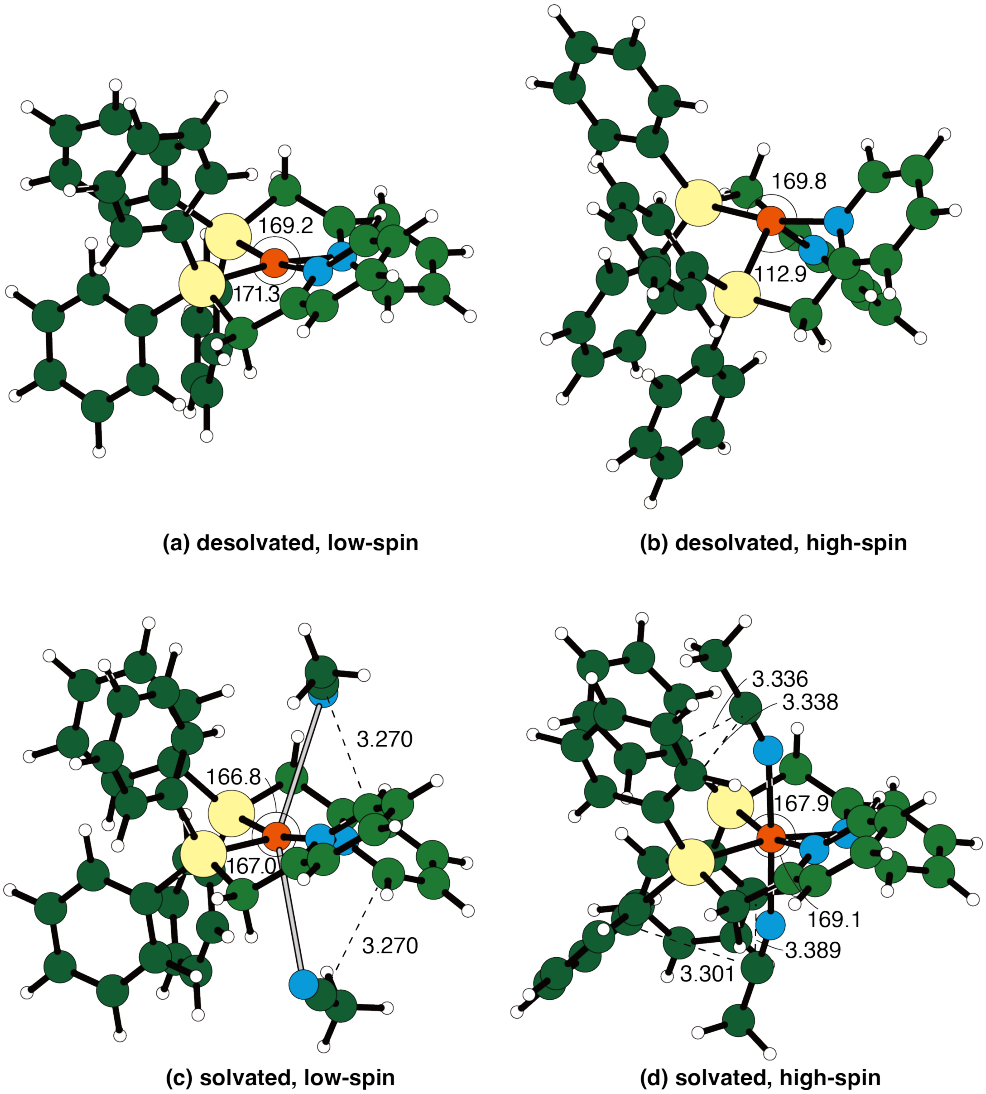

Fig. S14. The optimized structures of the desolvated $[Ni^{II}(L_H)_2]^{2+}$ in (a) the low- and (b) high-spin states and the MeCN-solvated $[Ni^{II}(L_H)_2(MeCN)_2]^{2+}$ in (c) the low- and (d) high-spin states. Red, yellow, blue, green, white circles denote Ni, P, N, C, and H atoms, respectively. Bond angles shown by arcs and the distances shown by dashed lines are in degrees and angstroms, respectively.

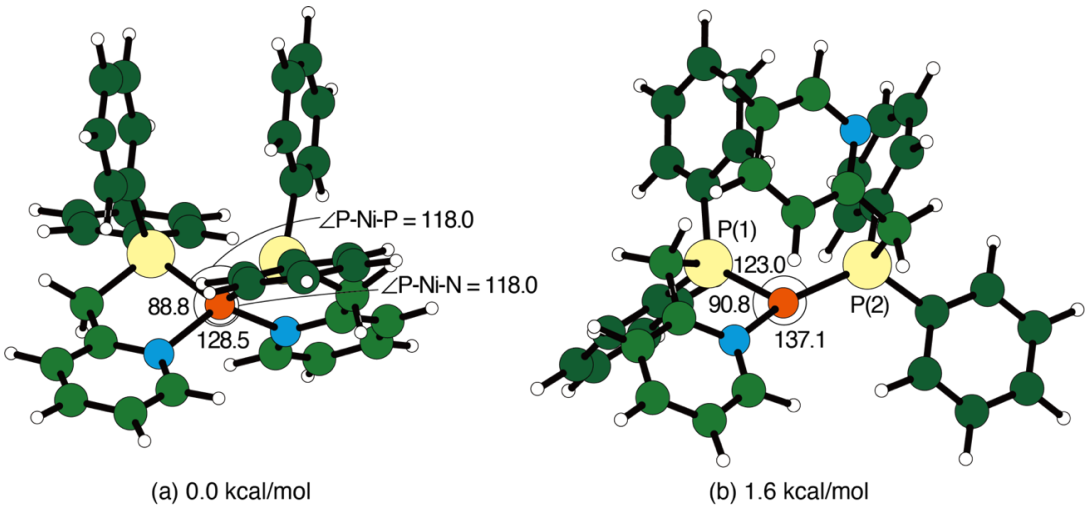

Fig. S15. The optimized structures of Ni(0) complex, $[Ni^{0}(L_H)_2]^{0}$, together with the relative energies in Gibbs free energy at 298.15 K. (a) The four-coordinated structure with bond lengths of Ni—P = 2.130 Å and Ni—N = 2.005 Å, respectively. (b) The three-coordinated structure with a free pyridyl group and bond lengths of Ni—P(1) = 2.119 Å, Ni—P(2) = 2.098 Å, and Ni—N = 1.936 Å. Color scheme is as in Fig. S14. Bond angles are in degrees.

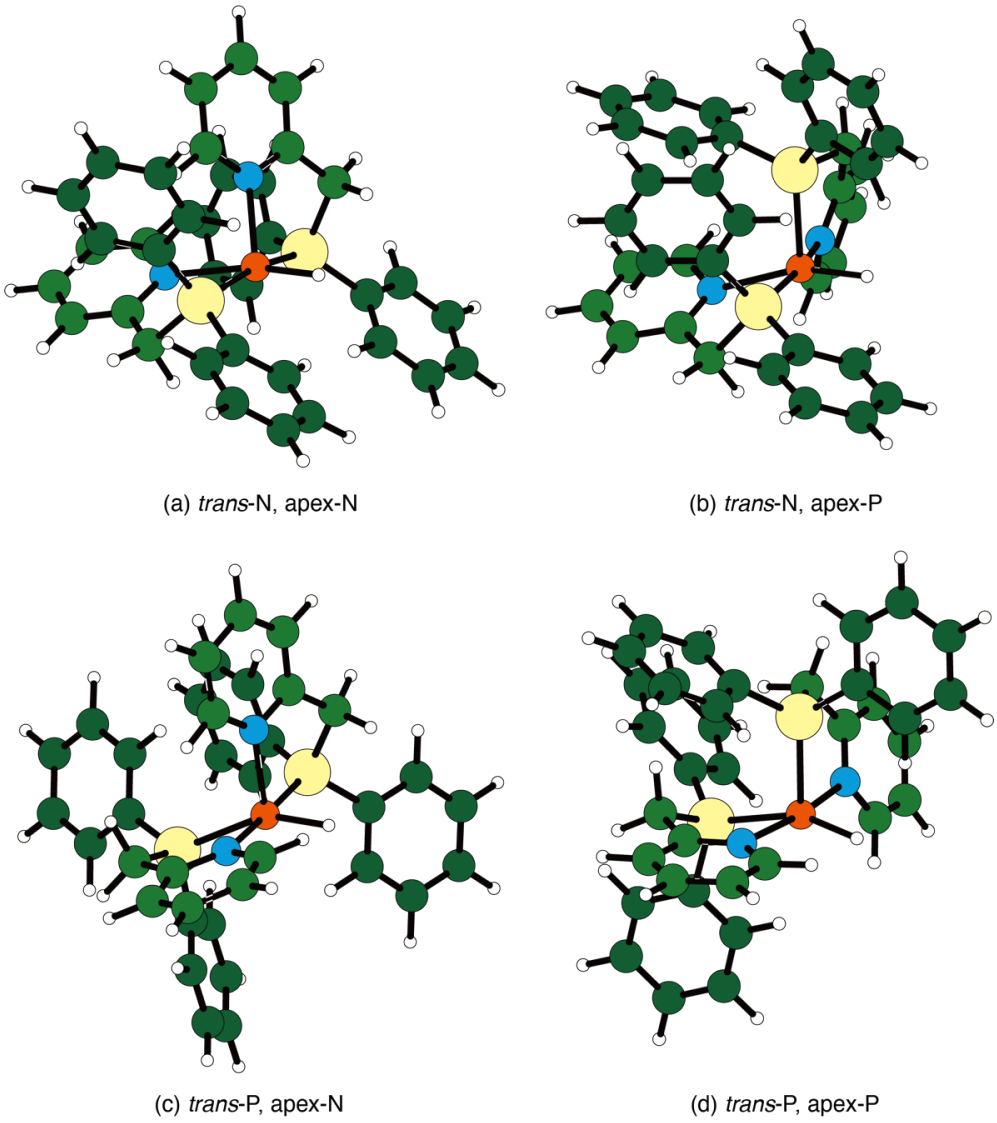

Fig. S16. The optimized structures of desolvated high-spin hydride Ni(II) complexes. Color scheme and classification of square pyramidal structures are as in Fig. S14.

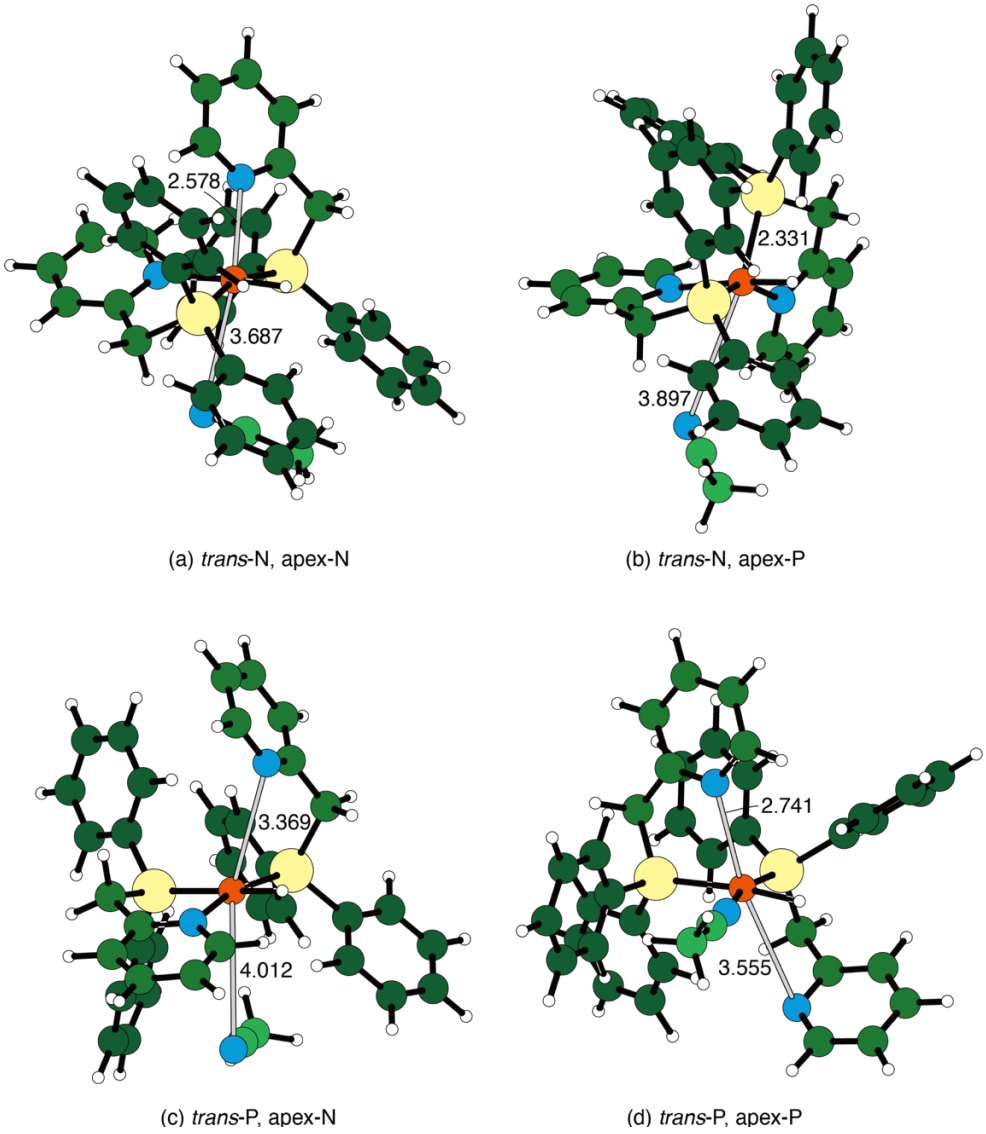

Fig. S17. The optimized structures of the mono-MeCN-solvated low-spin hydride Ni(II) complexes. Color scheme is as in Fig. S14. Gray sticks between donor atoms and Ni center represent distances longer than 2.5 Å. The distances are shown in Å. The labeling of the structures is the same as the original desolated analogues in Fig. S14, because the MeCN ligation, which occurs at the empty site of the desolated complexes, has no significant effect on the coordination geometry, except that some ligands are pushed away from the Ni centre.

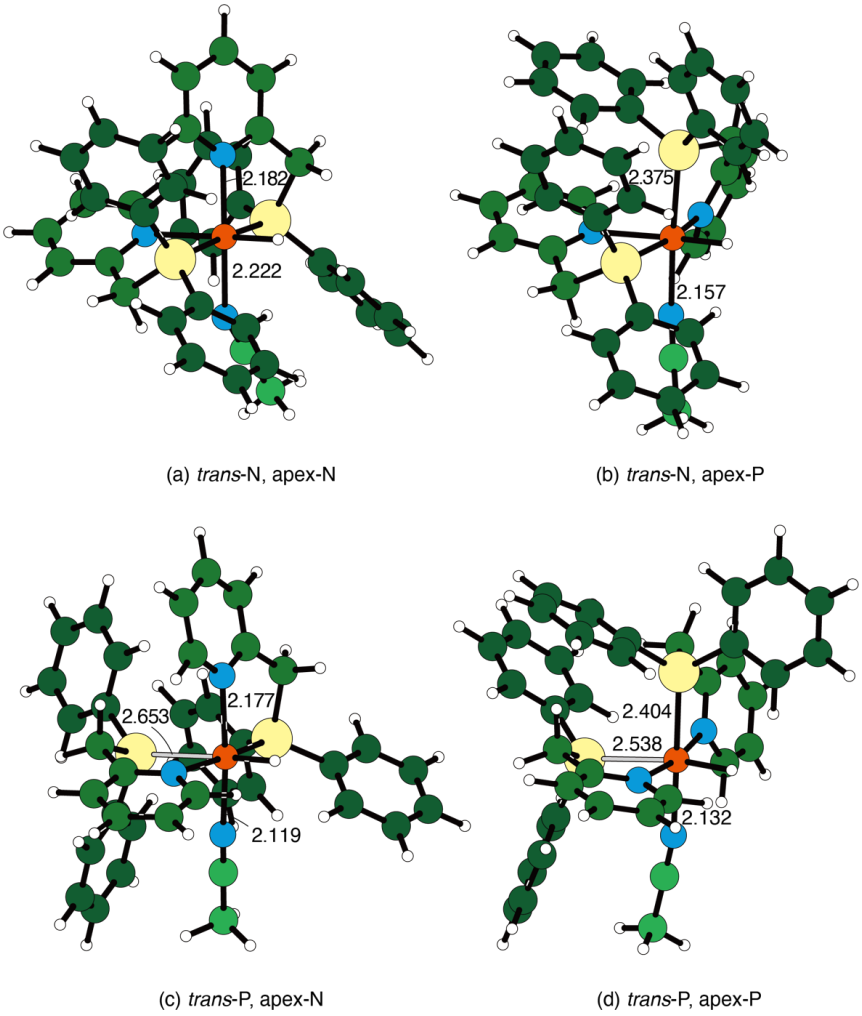

Fig. S18. The optimized structures of mono-MeCN-solvated high-spin hydride Ni(II) complexes. Color scheme and classification of square pyramidal structures are as in Fig. S14. The bond lengths are shown in Å.

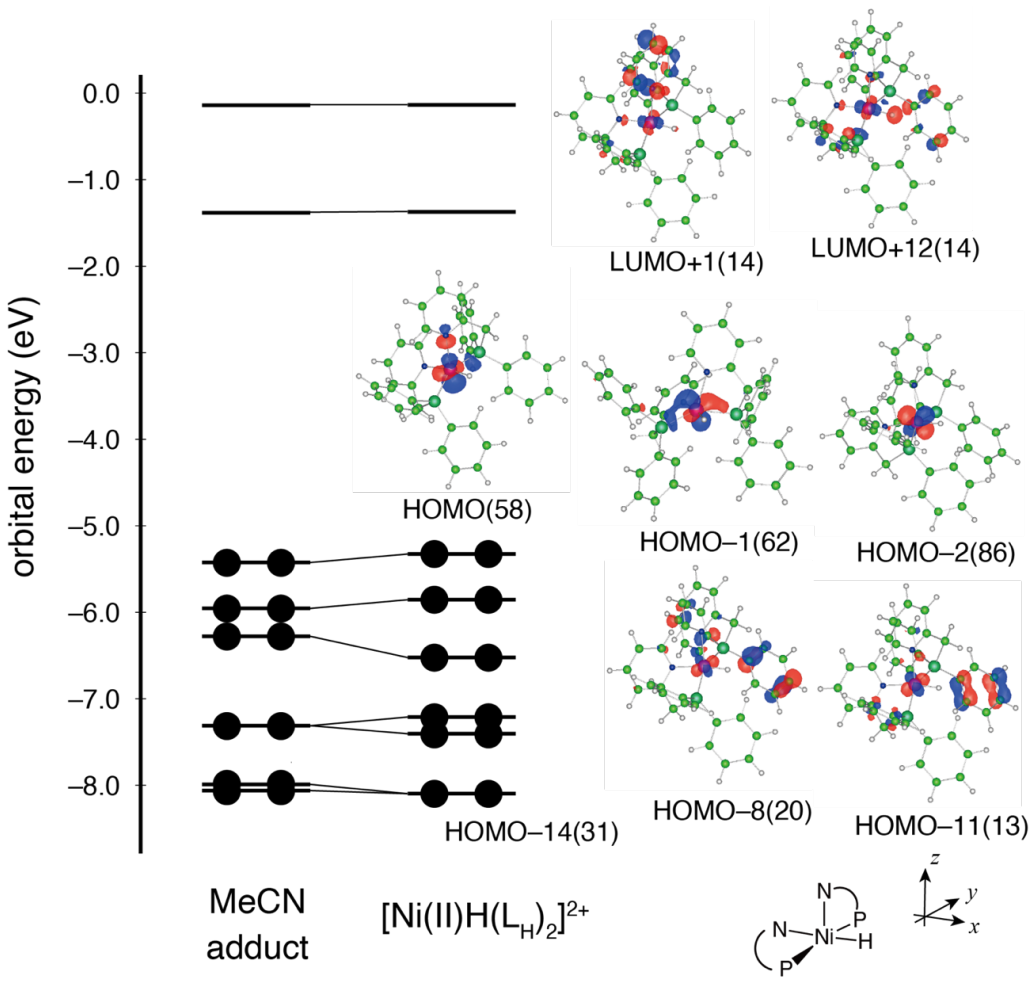

Fig. S19. Orbital energy level diagrams of the low-spin (*trans*-N, apex-N) hydride Ni(II) complex $[Ni^{II}H(L_H)_2]^{2+}$ (right side) and its mono-MeCN-solvated analogue (left side). The orbitals assigned to the d orbital on the Ni centre and the 1s orbital on the hydrido ligand are depicted. The values in parentheses indicate the percentage of d-orbital components. The orbital isosurfaces are ±0.06 a.u. The orbital diagram of the HOMO–14 is shown in Fig. S20(a). The splitting levels of orbital energies mean that the orbitals contain the same orbital component: e.g. the $3d_{xy}$ orbital on the Ni centre is mixed in the HOMO–8 and HOMO–11. Certain weights of the $d_{x^2-y^2}$ orbital are found in the LUMO+1 and LUMO+12.

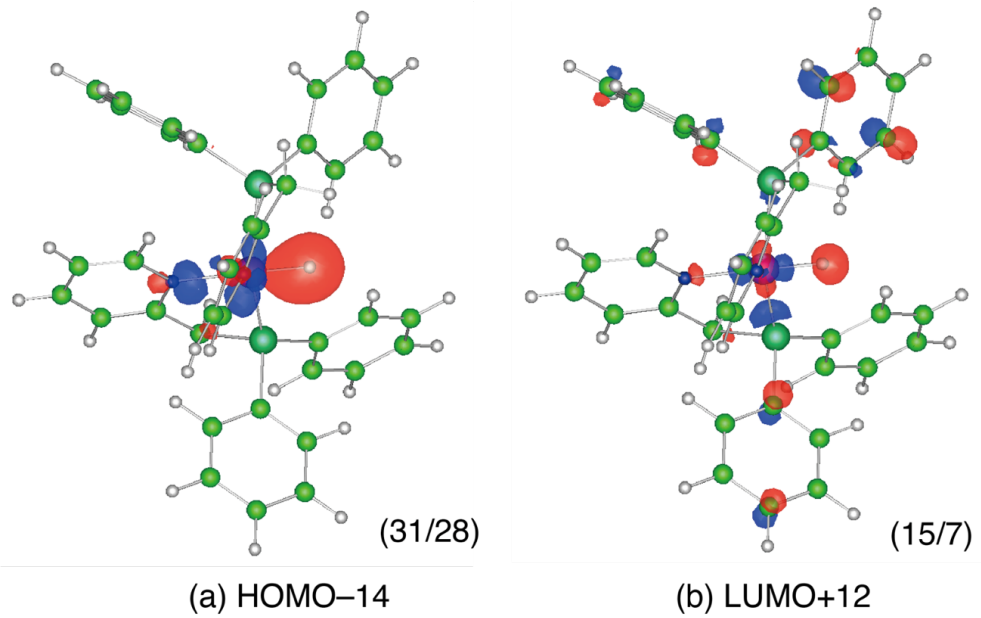

Fig. S20. The Ni—H (a) bonding and (b) antibonding orbitals. The values of orbital isosurfaces are ±0.06 a.u. The values in parentheses indicate the weight proportion of atomic orbitals in the Ni(3d) and H(1s) orbitals, for example (Ni(3d)/H(1s)).

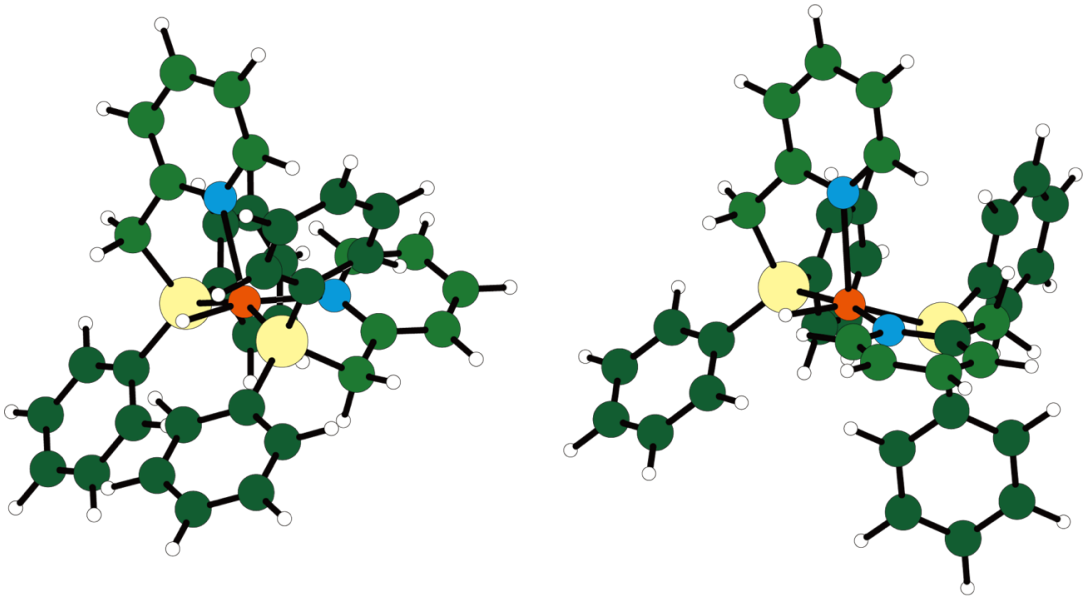

(a) *trans*-N, apex-N (b) *trans*-P, apex-N

Fig. S21. The optimized structures of the N-apex enantiomers of the desolvated low-spin hydride Ni(II) complexes. Color scheme and classification of square pyramidal structures are as in Fig. S14: (a) the enantiomer of Fig. 6(a), (b) the enantiomer of Fig. 6(c).

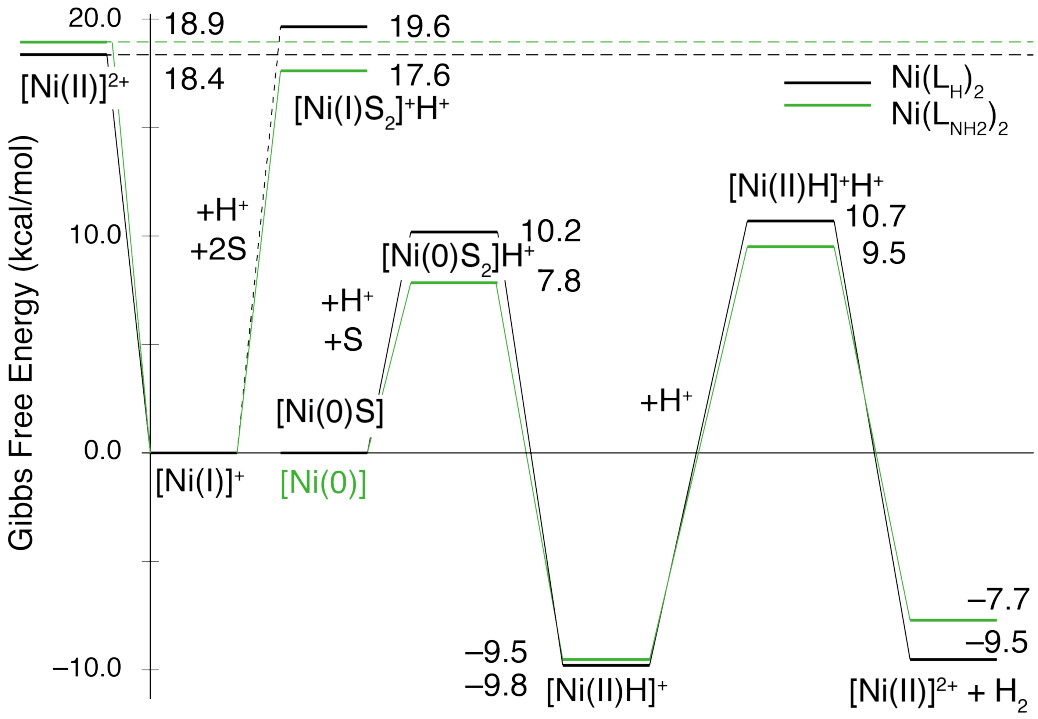

Fig. S22. The energy diagrams for the complex **1**, $[Ni^{II}(L_H)_2]^{2+}$, and $[Ni^{II}(L_{NH2})_2]^{2+}$ systems. The representation of species is as in Fig. 7. The free energy diagrams are plotted at an electrode potential equal to the Ni^I/Ni^0 reduction potential, and no free energy change for Ni^I/Ni^0 reduction. The dashed line connecting the potential energy levels for the protonation step of $[Ni^I(L_H)_2]^+$ represents a reaction step to the thermodynamically unfavorable product.

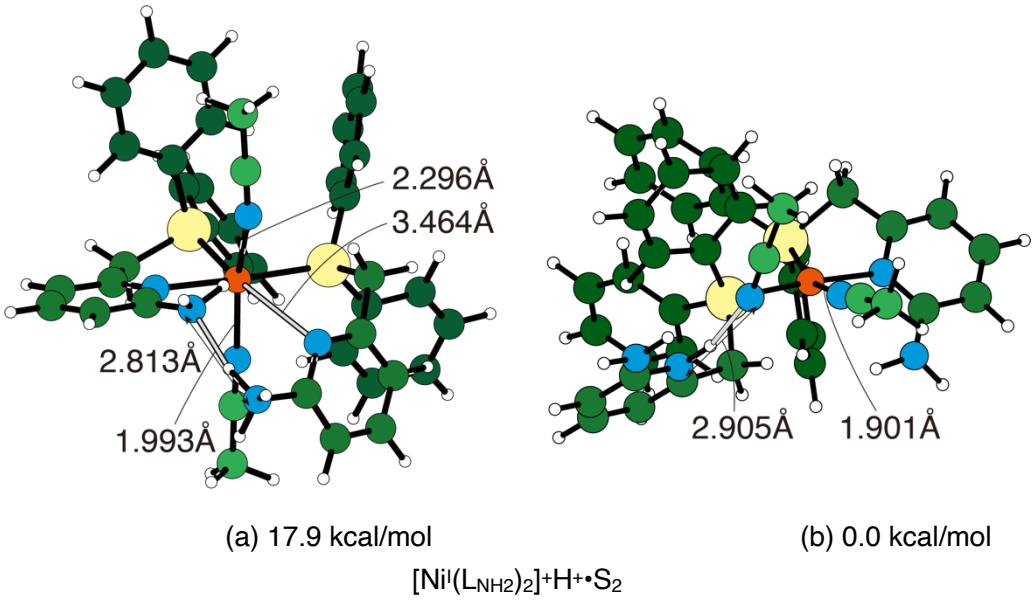

Fig. S23. Optimized structures of the protonated Ni(I) complex with two explicit solvent molecules for $[Ni^{II}(L_{NH2})_2]^{2+}$ systems: (a) an ammonium group forming an intramolecular H-bond to the amine group of the other ligand, (b) a pyridinium H-bonding to an MeCN molecule. Color scheme is as in Fig. S14, and formula symbols are as in Fig. 7. Gray bonds are H-bonds with distances between N atoms.

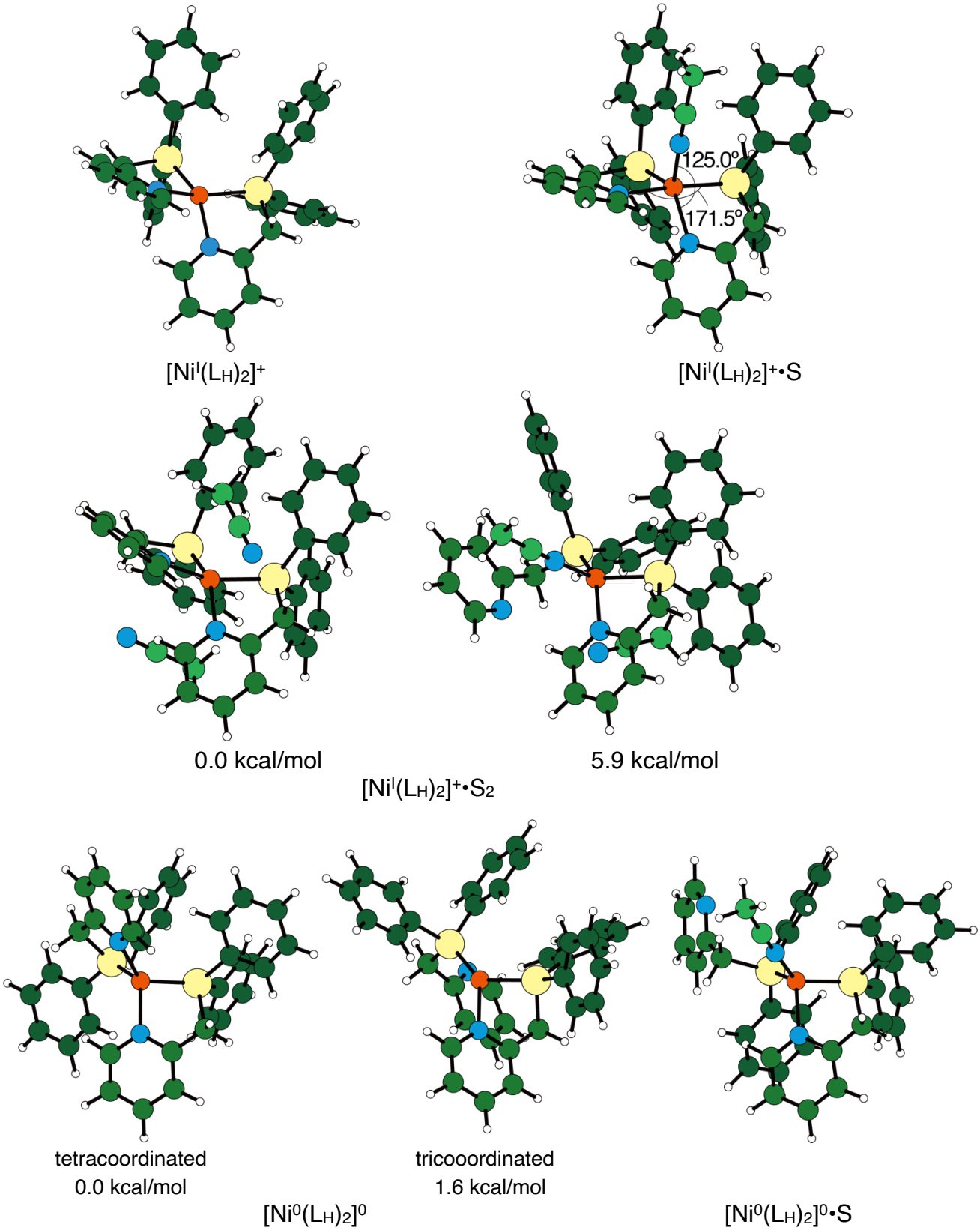

Fig. S24. Optimized structures of deprotonated complexes for [Ni^{II}(L$_H$)$_2$]$^{2+}$ systems. Color scheme is as in Fig. S14, and formula symbols are as in Fig. 7. Relative energies between isomers are shown.

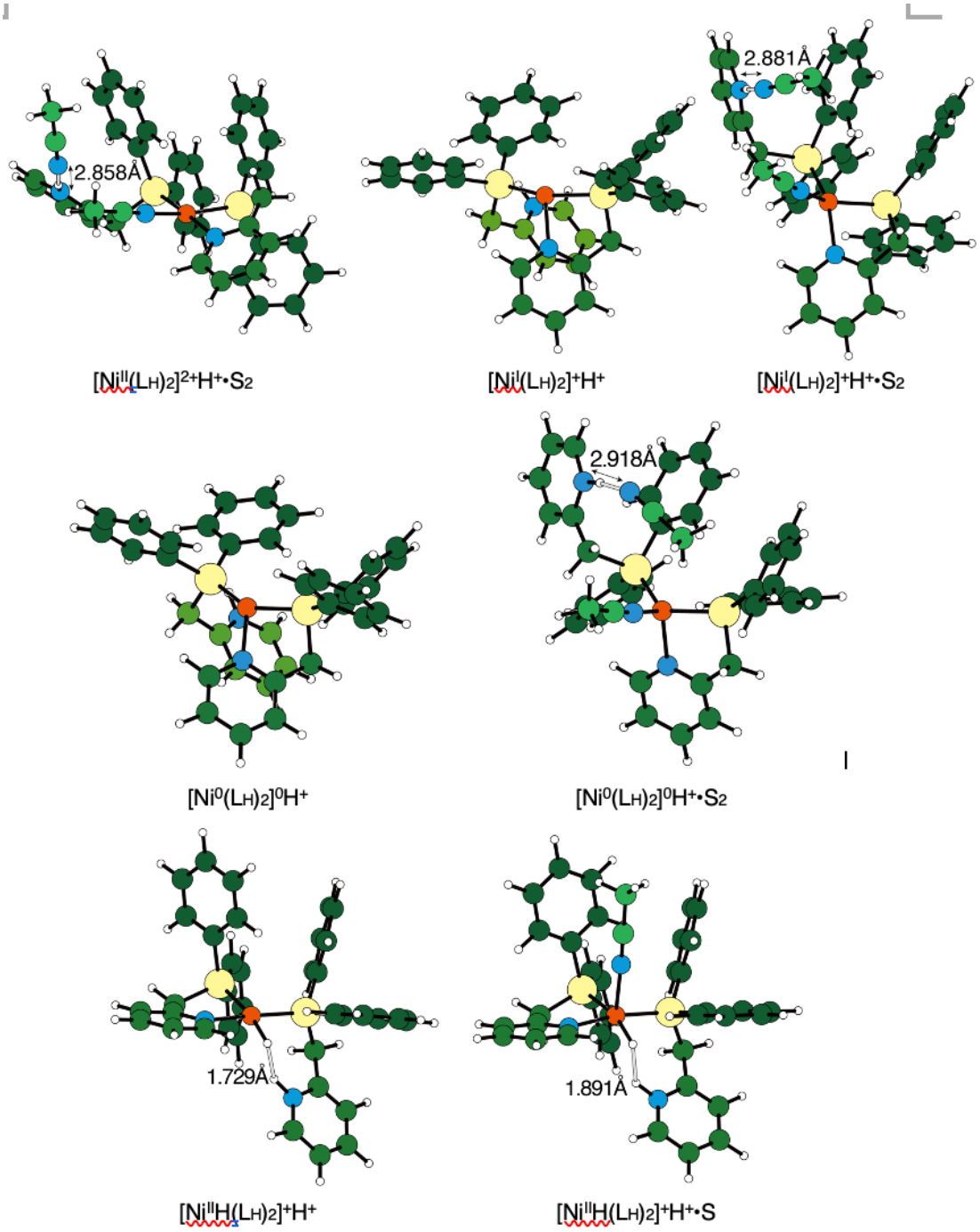

Fig. S25 Optimized structures of protonated complexes for $[Ni^{II}(L_H)_2]^{2+}$ systems. Color scheme as in Fig. S14 and formula symbols are as in Fig. 7. Gray bonds are hydrogen bonds with distances between N or H atoms for $[Ni^{II}(L_H)_2]^{2+}H^+$ and hydride complexes, respectively.

Table S1. Crystallographic details of $[Ni(L_H)_2](BF_4)_2$ (**1**)

Empirical Formula	$C_{36}H_{32}B_2F_8N_2NiP_2$
Formula Weight	786.92
Crystal System	orthorhombic
a /Å	24.171(2)
b /Å	27.647(2)
c /Å	10.3577(6)
V/Å^3	6921.6(7)
Space Group	*Fdd*2 (#43)
Z value	8
D_{calc}/g/cm^3	1.510
R1 (I>2.00s(I))	0.0216
R (All reflections)	0.0372
wR2 (All reflections)	0.0484
Goodness of Fit	0.972
Max Shift/Error	0.002

Table S2. Bond lengths (Å) and angles (deg) for [Ni($\mathbf{L_H}$)$_2$](BF$_4$)$_2$ (**1**)

atom	atom	distance	atom	atom	distance
Ni1	P1	2.1760(6)	Ni1	P11	2.1760(6)
Ni1	N1	1.952(2)	Ni1	N11	1.952(2)
P1	C3	1.835(3)	P1	C5	1.809(3)
P1	C7	1.803(3)	F2	B18	1.379(4)
F6	B18	1.371(4)	F10	B18	1.386(4)
F21	B18	1.361(4)	N1	C9	1.360(3)
N1	C16	1.347(3)	C3	C91	1.487(4)
C4	C7	1.398(4)	C4	C24	1.379(4)
C5	C11	1.391(3)	C5	C12	1.394(4)
C7	C8	1.395(4)	C8	C22	1.391(4)
C9	C19	1.378(4)	C11	C13	1.387(4)
C12	C14	1.383(4)	C13	C15	1.373(4)
C14	C15	1.383(4)	C16	C20	1.385(4)
C17	C19	1.382(4)	C17	C20	1.376(5)
C22	C23	1.369(5)	C23	C24	1.386(4)
C3	H3A	0.990	C3	H3B	0.990
C4	H4	0.950	C8	H8	0.950
C11	H11	0.950	C12	H12	0.950
C13	H13	0.950	C14	H14	0.950
C15	H15	0.950	C16	H16	0.950
C17	H17	0.950	C19	H19	0.950
C20	H20	0.950	C22	H22	0.950
C23	H23	0.950	C24	H24	0.950

atom	atom	atom	angle	atom	atom	atom	angle
P1	Ni1	P11	99.53(3)	P1	Ni1	N1	162.22(5)
P1	Ni1	N11	84.50(6)	P11	Ni1	N1	84.50(6)
P11	Ni1	N11	162.22(5)	N1	Ni1	N11	96.96(9)
Ni1	P1	C3	98.32(8)	Ni1	P1	C5	117.19(9)
Ni1	P1	C7	121.06(8)	C3	P1	C5	106.45(11)
C3	P1	C7	105.87(11)	C5	P1	C7	106.12(11)
Ni1	N1	C9	121.15(15)	Ni1	N1	C16	119.92(17)
C9	N1	C16	118.2(2)	P1	C3	C91	106.69(16)
C7	C4	C24	119.8(3)	P1	C5	C11	120.16(19)
P1	C5	C12	120.15(16)	C11	C5	C12	119.5(2)
P1	C7	C4	119.18(18)	P1	C7	C8	120.71(19)
C4	C7	C8	120.1(3)	C7	C8	C22	118.8(3)
N1	C9	C31	115.7(2)	N1	C9	C19	121.6(3)
C31	C9	C19	122.7(3)	C5	C11	C13	119.8(3)
C5	C12	C14	120.0(2)	C11	C13	C15	120.4(3)
C12	C14	C15	120.1(3)	C13	C15	C14	120.2(3)
N1	C16	C20	122.5(3)	C19	C17	C20	119.3(3)
C9	C19	C17	119.5(3)	C16	C20	C17	118.8(3)
C8	C22	C23	120.9(3)	C22	C23	C24	120.3(3)
C4	C24	C23	120.0(3)	F2	B18	F6	110.4(3)
F2	B18	F10	108.3(3)	F2	B18	F21	108.7(3)
F6	B18	F10	108.2(3)	F6	B18	F21	110.5(3)
F10	B18	F21	110.7(3)				
P1	C3	H3A	110.4	P1	C3	H3B	110.4
C91	C3	H3A	110.4	C91	C3	H3B	110.4
H3A	C3	H3B	108.6	C7	C4	H4	120.1
C24	C4	H4	120.1	C7	C8	H8	120.6
C22	C8	H8	120.6	C5	C11	H11	120.1
C13	C11	H11	120.1	C5	C12	H12	120.0
C14	C12	H12	120.0	C11	C13	H13	119.8
C15	C13	H13	119.8	C12	C14	H14	119.9
C15	C14	H14	120.0	C13	C15	H15	119.9
C14	C15	H15	119.9	N1	C16	H16	118.7
C20	C16	H16	118.8	C19	C17	H17	120.3
C20	C17	H17	120.4	C9	C19	H19	120.3

C17	C19	H19	120.2	C16	C20	H20	120.6
C17	C20	H20	120.6	C8	C22	H22	119.5
C23	C22	H22	119.5	C22	C23	H23	119.8
C24	C23	H23	119.8	C4	C24	H24	120.0
C23	C24	H24	120.0				

Table S3. Torsion angles (deg) for [Ni**L**$_2$](BF$_4$)$_2$ (**1**)

(Those having bond angles > 160 or < 20 degrees are excluded.)

atom1	atom2	atom3	atom4	angle
P1	Ni1	P11	C31	171.46(2)
P1	Ni1	P11	C51	58.07(3)
P1	Ni1	P11	C71	-74.29(4)
P11	Ni1	P1	C3	171.46(2)
P11	Ni1	P1	C5	58.07(3)
P11	Ni1	P1	C7	-74.29(4)
P1	Ni1	N11	C91	14.10(11)
P1	Ni1	N11	C161	-156.18(12)
N11	Ni1	P1	C3	-26.02(5)
N11	Ni1	P1	C5	-139.40(6)
N11	Ni1	P1	C7	88.23(6)
P11	Ni1	N1	C9	14.10(11)
P11	Ni1	N1	C16	-156.18(12)
N1	Ni1	P11	C31	-26.02(5)
N1	Ni1	P11	C51	-139.40(6)
N1	Ni1	P11	C71	88.23(6)
N1	Ni1	N11	C91	-148.07(12)
N1	Ni1	N11	C161	41.65(13)
N11	Ni1	N1	C9	-148.07(12)
N11	Ni1	N1	C16	41.65(13)
Ni1	P1	C3	C91	37.02(13)
Ni1	P1	C5	C11	71.91(18)
Ni1	P1	C5	C12	-103.31(16)
Ni1	P1	C7	C4	-176.78(11)
Ni1	P1	C7	C8	3.0(2)
C3	P1	C5	C11	-36.8(2)
C3	P1	C5	C12	147.95(17)
C5	P1	C3	C91	158.67(13)
C3	P1	C7	C4	-66.48(18)
C3	P1	C7	C8	113.30(17)
C7	P1	C3	C91	-88.69(15)
C5	P1	C7	C4	46.39(19)
C5	P1	C7	C8	-133.83(16)

C7	P1	C5	C11	-149.30(17)
C7	P1	C5	C12	35.5(2)
Ni1	N1	C9	C31	9.4(3)
Ni1	N1	C9	C19	-169.55(13)
Ni1	N1	C16	C20	170.83(13)
C9	N1	C16	C20	0.3(3)
C16	N1	C9	C31	179.83(17)
C16	N1	C9	C19	0.9(3)
P1	C3	C91	N11	-32.4(3)
P1	C3	C91	C191	146.54(16)
C7	C4	C24	C23	0.5(4)
C24	C4	C7	P1	-177.7(2)
C24	C4	C7	C8	2.5(4)
P1	C5	C11	C13	-176.06(17)
P1	C5	C12	C14	174.43(15)
C11	C5	C12	C14	-0.8(4)
C12	C5	C11	C13	-0.8(4)
P1	C7	C8	C22	176.56(16)
C4	C7	C8	C22	-3.7(4)
C7	C8	C22	C23	1.7(4)
N1	C9	C19	C17	-1.7(4)
C31	C9	C19	C17	179.45(19)
C5	C11	C13	C15	2.1(5)
C5	C12	C14	C15	1.2(4)
C11	C13	C15	C14	-1.7(5)
C12	C14	C15	C13	0.0(4)
N1	C16	C20	C17	-0.6(4)
C19	C17	C20	C16	-0.2(4)
C20	C17	C19	C9	1.3(4)
C8	C22	C23	C24	1.3(5)
C22	C23	C24	C4	-2.5(5)

ORTEP drawing of complex **1** with 50 % ellipsoid probability.

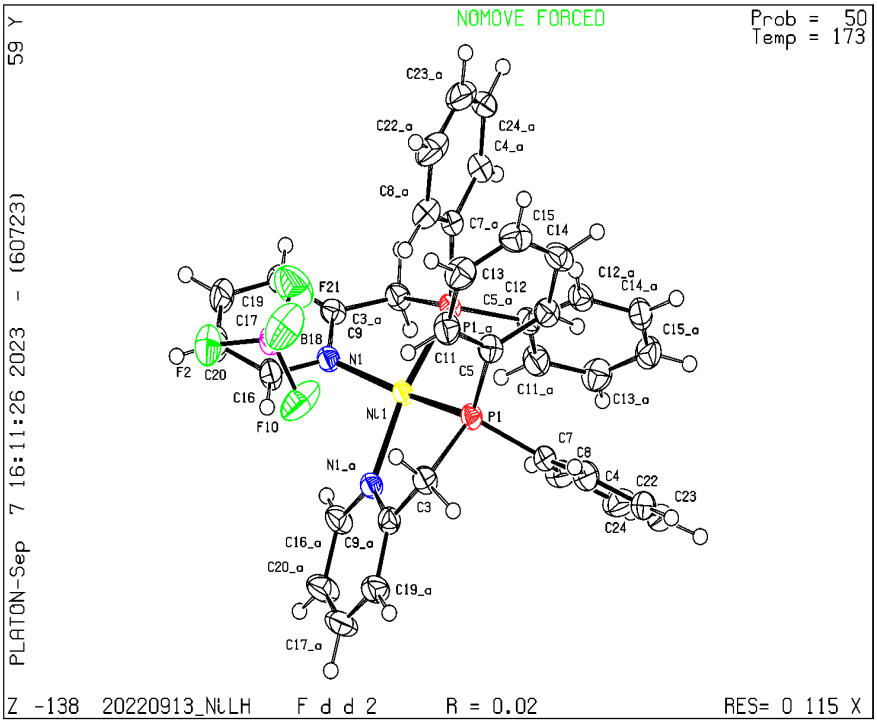

Table S4. Calculated solvation energies for species with and without protons for $[Ni^{II}(L_{NH2})_2]^{2+}$ and $[Ni^{II}(L_H)_2]^{2+}$ systems (kcal/mol).

		NH_2		H	
	coordination, spin state [a]	1	2	1	2
N(II) [b]	hexacoordinated, high-spin		3.1		1.3
	tetracoordinated, low-spin		1.0		1.6
Ni(I)	tetracoordinated	5.8	5.1	5.9	2.4
	leaving pyridyl		8.9		7.4
Ni(0)	leaving pyridyl	0.7		–0.7	
Ni(II)H	leaving pyridyl	1.5		0.1	
	protonated				
Ni(II) [b]	hexacoordinated, high-spin		–6.5		
	tetracoordinated, low-spin		–6.5		
	leaving ammoniumpyridyl		–8.6		
	leaving pyridinium		–20.7		
Ni(I)	pentacoordinated		10.3		
	leaving pyridinum		–7.5		–9.0
Ni(0)	leaving pyridinium		–3.4		–3.7
Ni(II)H	leaving pyridyl	2.4		4.5	

[a] The coordination number represents the number of donor atoms in the first coordination shell.

[b] The desolvated complex is in the low-spin state.

Table S5. Relative energies, Ni—H bond lengths, and natural atomic charges of hydride Ni(II) intermediates, $[Ni^{II}H(L_{NH2})_2]^+$.

trans atom of H^-	N		P	
apex atom	N	P	N	P
ΔG (kcal/mol)	1.0	2.6	0.0	9.7
Ni—H bond (Å)	1.457	1.457	1.486	1.500
atomic charge				
Ni	0.76	0.80	0.75	0.88
P	0.94	0.94	0.89[a]	0.90[a]
P	0.92	0.85[b]	1.01	0.83[b]
N	–0.63[a]	–0.64[a]	–0.62	–0.59
N	–0.63[b]	–0.65	–0.61[b]	–0.58
H	–0.23	–0.19	–0.30	–0.35

[a] at the trans position of the hydride ligand.

[b] at the apex position.